

Experiments on elastomechanical wave functions in chaotic plates and their statistical features

K. Schaadt,¹ T. Guhr,² C. Ellegaard,¹ and M. Oxborrow³

¹*Center for Chaos and Turbulence Studies, Niels Bohr Institute, Blegdamsvej 17, DK-2100 Copenhagen Ø, Denmark*

²*Matematisk Fysik, LTH, Lunds Universitet, Box 118, SE-22100 Lund, Sweden*

³*National Physical Laboratory, Teddington TW11 0LW, United Kingdom*

(Received 20 February 2003; published 5 September 2003)

We measure the amplitude of the elastomechanical displacement at a fine grid of points on a free plate having the shape of a Sinai stadium. The obtained displacement field formally corresponds to a wave function in a quantum system. While the distribution of the squared amplitudes agrees with the prediction of random matrix theory (RMT), there is a strong deviation of the spatial correlator from the standard prediction for quantum chaotic systems. We show that this is due to the presence of two modes, leading to a beating phenomenon. We construct a proper extension of the spatial correlator within the framework of RMT.

DOI: 10.1103/PhysRevE.68.036205

PACS number(s): 05.45.Mt, 43.20.+g

I. INTRODUCTION

Attracting interest in the field of quantum chaos, elastomechanical systems are being studied analytically, numerically, and experimentally. In 1989, Weaver measured the first few hundred eigenfrequencies of an aluminum block and worked out the spectral statistics [1]. The transition to chaos, symmetry breaking, and parametric level motion were measured in aluminum and quartz blocks [2–4]. For isotropic plates, important analytical results have been obtained by Bogomolny and Hugues using semiclassical methods [5]. Some of their results were confirmed in recent experiments [6,7]. In elastomechanical systems, first, the wave equation involves two types of wave motion (longitudinal and transverse) and, second, free boundary conditions apply in many cases. These two features make elastomechanical systems quite different from the often studied thin microwave cavities, which allow for an exact simulation of the two-dimensional Schrödinger equation; for reviews see Refs. [8,9]. Nevertheless, the spectral fluctuations of elastomechanical spectra are universal and follow the prediction of random matrix theory (RMT) for quantum chaotic systems [1–3]. It is our first goal to extend such investigations to the statistics of the elastomechanical displacement field, which we will refer to as a wave function from now on, because of the formal similarity to a quantum system. To this end, we study a freely vibrating isotropic plate of a certain shape which would, in the case of a quantum billiard, induce chaotic motion. Does RMT apply to elastomechanical wave functions as well? In this context, one should be aware that, in the parametric correlator [4], a statistically significant deviation was found, whose origin is, at present, still unclear. Our second goal is the study of the spatial correlator for the elastomechanical displacement field. As two modes are present in the system under study, the structure of the wave functions is much richer than in the previously studied microwave systems [10,11] (as analogs of quantum chaotic ones). Our system is also different from three-dimensional microwave cavities, where the distribution of frequency shifts, due to the presence of—effectively—random and independent electric and magnetic field components, was measured in Ref. [12]. Thus, we may expect new features for the spatial correlator in our experiment.

The paper is organized as follows. After briefly reviewing some properties of elastomechanical waves in Sec. II, we describe the experiment in Sec. III. In Sec. IV, we analyze the data and interpret our results. We present our conclusions in Sec. V.

II. SOME PROPERTIES OF ELASTOMECHANICAL WAVES

In a homogeneous and isotropic three-dimensional medium, elastomechanical waves obey the wave equation

$$\rho \frac{\partial^2 \mathbf{u}}{\partial t^2} = (\lambda + \mu) \nabla(\nabla \cdot \mathbf{u}) + \mu \nabla^2 \mathbf{u} \quad (1)$$

for the displacement vector \mathbf{u} . Here, λ and μ are the Lamé coefficients, ρ is the density, and we have assumed no external forces. For details, see, e.g., Ref. [13], and references therein. The Navier equation (1) is different from the scalar Schrödinger equation for a quantum particle in a two-dimensional domain both because it is vectorial and because the term $(\lambda + \mu) \nabla(\nabla \cdot \mathbf{u})$ is present. Equation (1) allows two types of wave motion: longitudinal and transverse. As pointed out by Berry [14], the vectorial character, implying the presence of different modes, formally relates elastomechanics to quantum mechanics for a particle with spin 1. In aluminum, longitudinal waves travel almost twice as fast as transverse waves. In the bulk, the two types of waves propagate independently. However, upon reflection at a boundary, *mode conversion* takes place: an incident wave that is purely longitudinal or transverse will, in general, give rise to *two* incident waves, one longitudinal and one transverse. Moreover, their angles of reflection are different (due to their different velocities), as described by Snell's law.

If we consider an infinite plate in the case where the shear wavelength is larger than twice the thickness of the plate, three classes of modes exist. The *flexural* modes (also called *bending* modes) are transverse modes that have displacement perpendicular to the plane of the plate. At low frequency, these are well described by the Kirchhoff-Love model [13], in which Eq. (1) reduces to the scalar biharmonic equation

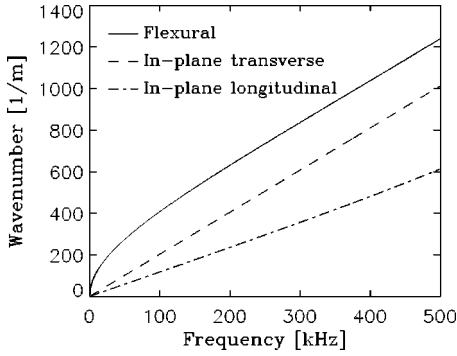


FIG. 1. The dispersion relations for the three types of modes in an infinite isotropic plate. We notice that, although the longitudinal waves are dispersive, the curvature is too small to be visible in the plot.

$$D\nabla^4 w + \rho h \frac{\partial^2 w}{\partial t^2} = 0. \quad (2)$$

Here, w is the vertical displacement, h is the thickness of the plate, and D denotes the *flexural rigidity*, given by $D = Eh^3/12(1-\nu^2)$, where E is Young's modulus and ν is Poisson's ratio; E and ν are functions of the Lamé coefficients [13].

Other modes have displacement in the plane of the plate and are labeled *in-plane*. These modes are studied in the Poisson model, where Eq. (1) reduces to a two-dimensional equation for the in-plane displacement vector

$$\rho \frac{\partial^2 \mathbf{u}}{\partial t^2} = \frac{E}{1+\nu} \left[\frac{1}{1-\nu} \nabla(\nabla \cdot \mathbf{u}) - \frac{1}{2} \nabla \times \nabla \times \mathbf{u} \right]. \quad (3)$$

The in-plane modes comprise two classes: *in-plane transverse* and *in-plane longitudinal*. The in-plane transverse modes obey the simple dispersion relation $k_t = 2\pi f/c_t$, where f is the frequency and c_t is the transverse velocity, i.e., these waves are nondispersive. Rayleigh and Lamb derived an exact, more complicated, dispersion relation for the flexural and in-plane longitudinal modes, see, e.g., Ref. [13]. The dispersion relations of models (2) and (3) serve as a guide for our experimental system; we will use the Rayleigh-Lamb dispersion relation later on to rescale our data. In Fig. 1, we show the dispersion relations for a plate of thickness 3 mm, Poisson's ratio 0.33, and transverse velocity 3100 m/s, which are the data for the plate used in recent experiments [6].

The statements made above strictly apply only to free wave propagation in infinite, uniform plates. For a finite plate, *mode conversion* takes place at the boundary. However, there is no mode conversion between the flexural and in-plane waves at plate edges because of the up/down symmetry at such edges. The side faces of our experimental plates were accurately machined such that this symmetry is preserved. Therefore, it is reasonable to expect that the flexural modes still comprise a single class of mode, uncoupled from any of the other mode types. This expectation was recently confirmed by experiment [6,7]. We also note that the flexural modes, being solutions to a scalar equation and not

influenced by mode conversion, represent the nearest elastomechanical analog to the transverse magnetic eigenmodes of a flat microwave cavity.

The in-plane waves, on the other hand, do undergo mode conversion at the boundary. The in-plane wave functions (i.e., standing waves) of a finite system will thus contain significant amounts of both types of wave motion [7], except for special geometries such as the rectangle where bouncing-ball states exist [15].

III. EXPERIMENT

The experimental setup is an extension of the one used in previous experiments [16]. We employ an HP 3589A spectrum/network analyzer to measure transmission spectra of elastomechanical resonators via piezoelectric transducers. The analyzer is run in scalar mode, implying that phases are not measured. In the present study, the elastomechanical resonator is an aluminum plate of thickness 3 mm, cut in the shape of a quarter Sinai stadium (the geometry introduced in Ref. [11]) with radii 29 mm and 50 mm. The new ingredient in the setup is a pickup, which can be accurately positioned using an (x,y) scanner, and which holds the receiving transducer. Thus, one can excite a single resonance peak in the transmission spectrum and measure its amplitude as a function of position \mathbf{R} on the plate. Scanning the surface of the plate in a fine grid then gives a measurement of the "amplitude landscape" of the wave function. The spatial resolution is 0.5 mm in each direction, which is much smaller than a typical wavelength of 10 mm. The pressure of the surrounding air is kept below 10^{-1} Torr, which reduces air damping to a level where the loss of elastomechanical energy is dominated by intrinsic losses and losses to the supports. The measurements are carried out at room temperature. The typical Q value of a resonance at 0.5 MHz (the typical frequency of a measured wave function) is 5×10^4 .

IV. DATA ANALYSIS AND INTERPRETATION

Regarding our choice of geometry, we are aware that the Sinai stadium billiard is known to be a mixed system, i.e., not completely chaotic. We emphasize, however, that the results presented here concern the elastomechanical wave equation with free boundaries, as opposed to the scalar Schrödinger equation and fixed boundaries of quantum billiards.

The statistics and the spatial correlations of the wave functions are discussed in Secs. IV A and IV B, respectively.

A. Wave function statistics

From the experimental results for the amplitude of the wave functions at the point \mathbf{R} in the Sinai stadium plate, we obtain the distributions of the normalized, squared amplitude $|\Psi(\mathbf{R})|^2$, which we shall refer to as *intensity* from now on. Figure 2 shows gray scale plots and distributions for three measured wave functions, two flexural (318.9 kHz and 425.1 kHz), and one in plane (510.6 kHz). Black represents maximum intensity, white represents zero intensity. Since the displacement vector is, for in-plane modes, not in general par-

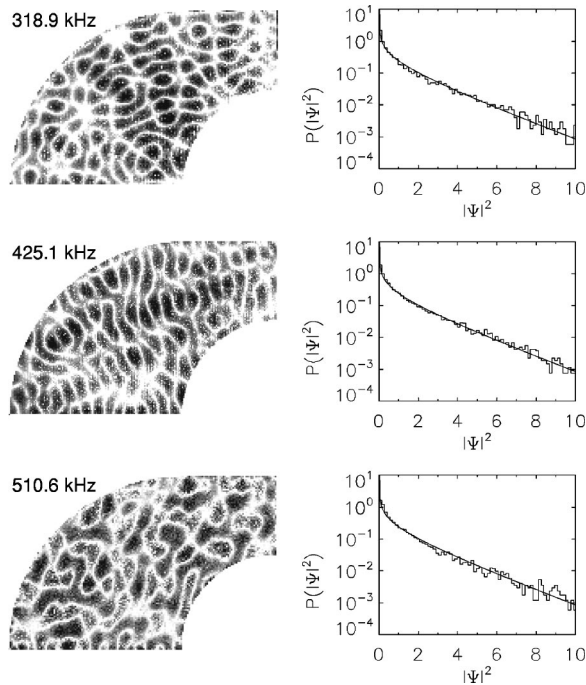


FIG. 2. Left: Grayscale plots for three measured wave functions; Two flexural modes (318.9 kHz and 425.1 kHz), and one in-plane mode (510.6 kHz). To enhance contrast, the grayscale is logarithmic. Black represents maximum intensity, white is zero intensity. One notes the complexity of the white structures, usually referred to as *nodal lines*. Right: Plots showing probability distribution for the intensity, corresponding to each mode. The step function represents the measurement while the solid line is the Porter-Thomas distribution. Note the \log_{10} -scale on the secondary axis.

allel to the polarization of the piezo device, we measure an effective projection of its full distribution. For a chaotic geometry, the distribution of the intensities $|\Psi(\mathbf{R})|^2$ is expected to follow the Porter-Thomas law,

$$P(|\Psi(\mathbf{R})|^2) = \frac{1}{2\sqrt{2\pi}|\Psi(\mathbf{R})|^2} \exp\left(-\frac{|\Psi(\mathbf{R})|^2}{2}\right), \quad (4)$$

see the reviews in Refs. [8,17]. As Fig. 2 demonstrates, we find excellent agreement with the expected distribution for flexural and in-plane modes. Note that, in our analysis, we decided to exclude points close to the plate's perimeter, because such a free boundary is known to lead to a behavior of the wave functions which would not be covered by Porter-Thomas statistics. This is due to exponential, i.e., nonoscillatory solutions of the biharmonic equation (2) for the flexural modes; for a discussion see Ref. [5]. These solutions describe a “flapping” of the plate, which only occurs within a distance of the order of $1/k$ from the perimeter.

Closer inspection of the wave functions in Fig. 2 reveals a smattering of individual pixels that are significantly lighter than their immediate surroundings; these are most noticeable within dark regions of near-to-maximum intensity. We interpret such pixels as “dropouts,” arising from poor contact between the scanning transducer and the plate, presumably due to microscopic irregularities in the plate's surface (such

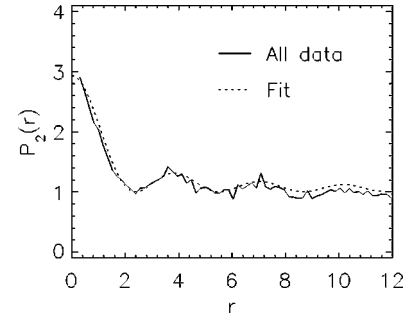


FIG. 3. Comparison of flexural data and RMT for the correlation function $P_2(r) = 1 + bJ_0^2(r)$. The solid curve represents an average over four measured flexural standing waves, while the dashed curve is a fit to these data yielding $b = 1.93 \pm 0.05$.

as scratches or pits). As any attempt to correct for such dropouts would involve arbitrary judgment, we elect to work with the raw data as shown. Note that the spatial distribution of the dropouts is uncorrelated with the wave function pattern in all cases. The inclusion of these dropouts in our analysis causes a small transfer of weight in the intensity distribution from high-intensity to lower-intensity regions, but the effect is not perceptible. All three intensity distributions in Fig. 2 show good agreement with the Porter-Thomas distribution over several decades.

B. Intensity correlator

To obtain information about spatial correlations, one could measure the wave function correlator. However, as our setup does not yield phase information, we decide to use the spatial intensity correlator $P_2(R)$, which relates intensities at points \mathbf{R}_1 and \mathbf{R}_2 ,

$$P_2(R) = \langle |\Psi(\mathbf{R}_1)|^2 |\Psi(\mathbf{R}_2)|^2 \rangle, \quad (5)$$

where the brackets denote average over the mean positions $(\mathbf{R}_1 + \mathbf{R}_2)/2$. As this also eliminates angular dependence, the correlator is only a function of the distance $R = |\mathbf{R}_1 - \mathbf{R}_2|$. The Bessel function character of such correlators was shown in Refs. [18,19], see Refs. [20,21]. One has

$$P_2(r) = 1 + 2J_0^2(r), \quad (6)$$

with J_0 denoting the zeroth-order Bessel function. Here, we introduced the dimensionless distance $r = kR$, where k is the wave number. When parts of the phase space are regular, corrections are needed [22], as were measured by Kudrolli *et al.* [11] in a microwave billiard with disorder. In Fig. 3, we present our result for correlator (5) of flexural wave functions. Here, we average over four separate wave functions, two of which are shown in Fig. 2. To work out correlator (5) for a measured flexural wave function, we calculate the wave number k from the frequency, using the appropriate expansion of the dispersion relation for wave propagation along the corresponding infinite, uniform plate. We replace the constant factor of 2 in formula (6) with a variable b , which we fit to the experimental data. We obtain $b = 1.93 \pm 0.05$. Thus, we find agreement between the experimental data and

the RMT prediction—as expected because of the agreement with the Porter-Thomas distribution found above.

We now address the in-plane modes. It will turn out that the simple form (6) of the correlator is completely destroyed. The reason is the presence of two modes. We calculate a prediction for the spatial correlator. To this end, we extend Srednicki's approach [23] which builds upon Berry's conjecture [18]. We write the wave function as the sum of two waves, e.g., a longitudinal one $\Psi_l(\mathbf{R})$ and a transverse one $\Psi_t(\mathbf{R})$,

$$\Psi(\mathbf{R}) = a_l \Psi_l(\mathbf{R}) + a_t \Psi_t(\mathbf{R}), \quad (7)$$

where the longitudinal and the transverse wave vectors \mathbf{k}_l and \mathbf{k}_t are different. We assume no phase shifts. The coefficients a_l and a_t determine the relative weights. We want to calculate correlator (5) for superposition (7) at two different points \mathbf{R}_1 and \mathbf{R}_2 . We assume that the wave functions $\Psi_x(\mathbf{R}_i)$ with $x=l,t$ and $i=1,2$ are multivariate Gaussian distributed according to

$$P \sim \exp\left(-\frac{1}{2} \sum_{x,y,i,j} \Psi_x(\mathbf{R}_i) [M^{-1}]_{xyij} \Psi_y(\mathbf{R}_j)\right). \quad (8)$$

The matrix M is real symmetric and has as elements the averages

$$\begin{aligned} M_{lilj} &= \langle \Psi_l(\mathbf{R}_i) \Psi_l(\mathbf{R}_j) \rangle = f_l(R), \\ M_{titi} &= \langle \Psi_t(\mathbf{R}_i) \Psi_t(\mathbf{R}_j) \rangle = f_t(R), \\ M_{litj} &= \langle \Psi_l(\mathbf{R}_i) \Psi_t(\mathbf{R}_j) \rangle = f_{lt}(R), \end{aligned} \quad (9)$$

combining the longitudinal and the transverse wave with itself and the two of them with one another. The functions f_l , f_t and f_{lt} depend only on the distance R between the two points. Normalization requires that we have $f_l(0)=1$ and $f_t(0)=1$. There is no such condition on f_{lt} . We note that we may normalize to unit volume or, in this case, to unit area. Due to the Gaussian assumption (8), correlator (5) can be calculated in a straightforward manner. The result is

$$\begin{aligned} P_2(R) &= [a_l^2 f_l(0) + 2a_l a_t f_{lt}(0) + a_t^2 f_t(0)]^2 + 2[a_l^2 f_l(R) \\ &\quad + 2a_l a_t f_{lt}(R) + a_t^2 f_t(R)]^2. \end{aligned} \quad (10)$$

This can easily be extended to an arbitrary number of modes. For the functions f_l and f_t in correlator (10), we may insert Berry's formula [18] for a two-dimensional system, yielding $f_l(R) = J_0(k_l R)$ and $f_t(R) = J_0(k_t R)$ with $k_l = |\mathbf{k}_l|$ and $k_t = |\mathbf{k}_t|$. We assume that the longitudinal and the transverse waves are statistically uncorrelated such that $f_{lt}(R) = 0$. For consistency reasons we should also have the normalization $a_l^2 + a_t^2 = 1$. Hence, we arrive at the correlator

$$P_2(R) = 1 + 2[a_l^2 J_0(k_l R) + a_t^2 J_0(k_t R)]^2, \quad (11)$$

which we compare to our experimental data. Figure 4 shows an average over 21 measured in-plane wave functions, measured in the frequency range from 450 kHz to 510 kHz. To compare with prediction (11), we find it convenient to nor-

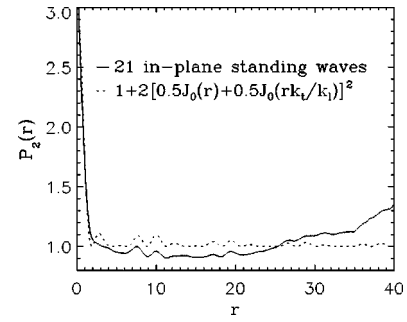


FIG. 4. Comparison of in-plane data and RMT for the correlation function $P_2(r)$ given by Eq. (11) with $a_l^2 = a_t^2 = 0.5$. The solid curve represents an average over 21 measured in-plane standing waves, while the dashed curve is the random matrix model. We note that $r = k_l R$ is the dimensionless distance, where R is the distance.

malize the experimental and theoretical result to the longitudinal wave number k_l , thereby introducing the dimensionless distance $r = k_l R$. Figure 1 shows that the dispersion relation for transverse waves is exactly linear and for longitudinal waves linear to a very good approximation in the frequency range considered. Therefore, the ratio k_l/k_t remains constant, and no new scale is introduced by averaging over different in-plane wave functions.

The difference between the result here and the case discussed above, with one type of wave motion, is striking. The presence of two modes leads to a beating phenomenon resulting in a much less pronounced structure in the correlator with only some isolated bumps. The interference responsible for this behavior comes in through the measurement, where the components of the transverse and the longitudinal displacement fields are projected onto a real number, which is the voltage produced by the piezoelectric component.

For intermediate R , the theoretical prediction (11) describes the shape of the experimental result well, in particular the bumps in the correlator. Since we cannot infer the above mentioned projection quantitatively from our data, we adjust the constants a_l and a_t in the predicted correlator (11) in such a way that these bumps are reproduced in the best possible way. This led us to put $a_l^2 = a_t^2 = 0.5$. Although the above mentioned projection is not precisely known, we are still able to justify the approximate size of these numbers. We know from independent calibration that our receiving transducer is about three times more sensitive to pure out-of-plane motion than to pure in-plane motion. The ratio of longitudinal energy to shear energy is $\kappa^2 = c_l^2/c_t^2 \approx 3$ for a plate, where $c_l = \kappa c_t = \sqrt{(2/1-\nu)} c_t$ is the plate-longitudinal velocity. Assuming that the vibrational energy density is proportional to the squared wave velocity and to the squared amplitude of vibration, and using that the out-of-plane amplitude associated with the longitudinal wave is just ν times the longitudinal in-plane displacement, we find that $(V_{l1} + V_{l2})/V_t \approx 2/3$, where the V 's represent expected, measured voltages associated with the amplitudes of the two longitudinal displacements and the transverse displacement, respectively. We emphasize that this is a rough estimate. We also note that the relative coupling of the transmitting transducer to the two wave types is of no importance in this

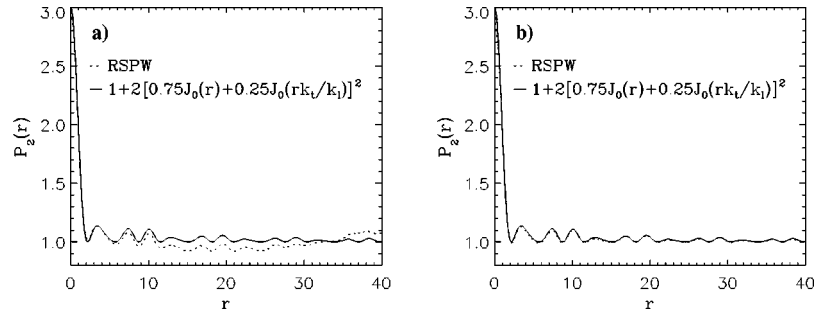


FIG. 5. Comparison of numerical data and RMT for the correlation function $P_2(r)$ given by Eq. (11) with $a_l^2=0.75$ and $a_t^2=0.25$. The solid curve represents the random matrix model, while the dashed curve is the random superposition of plane waves. The numerical results are calculated for two situations: A small system with just six longitudinal wavelengths across the system (a), resembling the experimental situation, and a big system with 50 longitudinal wavelengths across the system (b).

context. For a chaotic system such as the Sinai stadium, mode conversion distributes the energy to the equilibrium values within a few reflections. This should be compared to the lifetime of the wave, which spans thousands of reflections.

As for the global structure of the correlator, there is first an undershoot between $r=5$ and $r=25$, and second an overshoot for larger r . This can be understood if one takes into account, first, the finiteness of our system and, second, the boundary conditions. To demonstrate how the undershoot comes about, we present numerical simulations for a random superposition of plane waves, where the wave numbers were chosen to be the same as those in the experiment. Figures 5(a) and 5(b) show the results for a small and for a large system, respectively, compared to the theoretical prediction (11). In Figures 5(a) and 5(b) we have chosen different values for a_l and a_t compared to Fig. 4, in order to give an impression of how the correlator depends on these two coefficients. While the resulting correlator in the larger system agrees perfectly with the theory, there is an undershoot visible for the small system, exactly of the type found in the experiment which was of the same size. Although the simulation for the small system does show an overshoot, it is much smaller than observed in the experiment. Thus, we conclude that the experimental result for larger values of r reflects the free boundary conditions in our experiment. Similar to the flexural modes, discussed in Sec. IV A, the in-plane modes also have systematic excess amplitudes in the boundary region. Hence, at distances R which are comparable to the size of the plate, this contributes to the correlator. In our numerical simulation, the amplitudes at the boundary are random and therefore do not affect the correlator. Of course, these excess amplitudes will also influence the correlator at distances R comparable to $1/k$. In our opinion, this explains why the structure consisting of the dip near $r=2$ followed by the bump near $r=3$ in the RMT prediction is washed out and thus not visible in the measured correlator. We do not contribute the undershoot of the correlator in the intermediate range to this effect just discussed, rather we believe it is due to the finiteness of the system, as explained above.

The existence of scanning dropouts in the measured wave functions, as already mentioned in Sec. IV A, adds some

noise to the spatial correlators shown in Figs. 3 and 4. We can only expect, however, to reveal the RMT prediction by averaging over an ensemble of the correlators for several individual wave functions. Thus, the noise injected due to the shortcomings of our experiment is indistinguishable from and simply adds to the ensemble noise, i.e., to the one from the scattering around the averaged result. The experimental correlator in Fig. 4 is remarkably smooth. We interpret this as an indication that the noise stemming from the presence of dropouts is marginal compared to the ensemble noise.

V. CONCLUSIONS

We have conducted an experimental study of the wave function statistics of the flexural and in-plane modes of a Sinai stadium shaped aluminum plate. For flexural modes, the wave equation reduces to a scalar biharmonic equation, whereas in-plane modes are solutions to a vectorial wave equation. In the latter case, the wave equation is qualitatively different from the Schrödinger equation for a quantum particle in a two-dimensional domain. We find accurate agreement with RMT for the two quantities under study: the distribution of intensity for both mode types and a spatial correlation for the flexural modes. As for the flexural modes, our results for the distribution and spatial correlation of intensity show, for elastomechanical systems, that the universal predictions of RMT are valid not only for the spectral fluctuation statistics, as found in Ref. [1–3], but also for properties of the wave functions. As this statement applies to waves described by a biharmonic, i.e., fourth-order equation, the statistical model of RMT is experimentally proven to be robust also in this respect.

Moreover, we have, by investigating a system with two different types of modes, demonstrated that the spatial correlator (6) for one type of wave is a somewhat fragile quantity. If another type of wave mixes in, the pronounced oscillatory structure is destroyed due to a beating phenomenon. We believe that this will also be relevant in many complex quantum systems where different classes of modes are present. In molecules, for example, one is confronted with exactly such a situation, as becomes obvious in the Born-Oppenheimer approximation, which leads to a Hamiltonian that explicitly contains such different classes of modes.

Note added. After completion of this work, we became aware of a recent similar investigation by Doya *et al.* [24] who studied speckle statistics in optical fibers. Reference [25] contains a derivation of correlator (11) and a comparison with data measured in optical fibers.

ACKNOWLEDGMENTS

We acknowledge fruitful discussions with A. D. Jackson and P. Bertelsen. This work was supported by the Danish and Swedish National Research Councils.

-
- [1] R.L. Weaver, J. Acoust. Soc. Am. **85**, 1005 (1989).
 - [2] C. Ellegaard, T. Guhr, K. Lindemann, H.Q. Lorensen, J. Nygård, and M. Oxborrow, Phys. Rev. Lett. **75**, 1546 (1995).
 - [3] C. Ellegaard, T. Guhr, K. Lindemann, J. Nygård, and M. Oxborrow, Phys. Rev. Lett. **77**, 4918 (1996).
 - [4] P. Bertelsen, C. Ellegaard, T. Guhr, M. Oxborrow, and K. Schaadt, Phys. Rev. Lett. **83**, 2171 (1999).
 - [5] E. Bogomolny and E. Hugues, Phys. Rev. E **57**, 5404 (1998).
 - [6] P. Bertelsen, E. Hugues, and C. Ellegaard, Eur. Phys. J. B **15**, 87 (2000).
 - [7] A. Andersen, C. Ellegaard, A.D. Jackson, and K. Schaadt, Phys. Rev. E **63**, 066204 (2001).
 - [8] T. Guhr, A. Müller-Groeling, and H.A. Weidenmüller, Phys. Rep. **299**, 189 (1998).
 - [9] H.J. Stöckmann, *Quantum Chaos—An Introduction* (Cambridge University Press, Cambridge, 1999).
 - [10] H. Alt, H.D. Gräf, H.L. Harney, R. Hofferbert, H. Lengeler, A. Richter, P. Schardt, and H.A. Weidenmüller, Phys. Rev. Lett. **74**, 62 (1995).
 - [11] A. Kudrolli, V. Kidambi, and S. Sridhar, Phys. Rev. Lett. **75**, 822 (1995).
 - [12] U. Dörr, H.J. Stöckmann, M. Barth, and U. Kuhl, Phys. Rev. Lett. **80**, 1030 (1998).
 - [13] K.F. Graff, *Wave Motion in Elastic Solids* (Dover, New York, 1975).
 - [14] M. V. Berry (unpublished).
 - [15] K. Schaadt, G. Simon, and C. Ellegaard, Phys. Scr., T **T90**, 231 (2001).
 - [16] M. Oxborrow and C. Ellegaard, in *Proceedings of the Third International Conference on Experimental Chaos*, edited by R.G. Harrison *et al.* (World Scientific, Singapore, 1996), p. 251.
 - [17] Fritz Haake, *Quantum Signatures of Chaos*, 2nd ed. (Springer-Verlag, Heidelberg, 2001).
 - [18] M.V. Berry, J. Phys. A **10**, 2083 (1977).
 - [19] M. Rollwage, K.J. Ebeling and D. Guicking, Acustica **58**, 149 (1985).
 - [20] V.N. Prigodin, B.L. Altshuler, K.B. Efetov and S. Iida, Phys. Rev. Lett. **72**, 546 (1994).
 - [21] Y.V. Fyodorov and A.D. Mirlin, Phys. Rev. B **51**, 13 403 (1995).
 - [22] A.D. Mirlin and Y.V. Fyodorov, J. Phys. A **26**, L551 (1993).
 - [23] M. Srednicki, Phys. Rev. E **54**, 954 (1996).
 - [24] V. Doya, O. Legrand, F. Mortessagne, and C. Miniatura, Phys. Rev. E **65**, 056223 (2002).
 - [25] V. Doya, Ph.D. thesis, Université de Nice, 2000.